Conformations and Structures of Poly(oxyethylene) Melts from Molecular Dynamics Simulations and Small-Angle Neutron Scattering Experiments

Grant D. Smith*

Department of Chemical Engineering, University of Missouri—Columbia, Columbia, Missouri 65211

Do Y. Yoon*

IBM Research Division, Almaden Research Center, 650 Harry Road, San Jose, California 95120

Richard L. Jaffe

STC 230-3, NASA Ames Research Center, Moffett Field, California 94035

Ralph H. Colby

Department of Materials Science and Engineering, The Pennsylvania State University, University Park, Pennsylvania 16802

Ramanan Krishnamoorti

Department of Materials Science and Engineering, Cornell University, Ithaca, New York 14853

Lewis J. Fetters

Exxon Research and Engineering Company, Corporate Research, Annandale, New Jersey 08801

Received October 30, 1995; Revised Manuscript Received February 1, 1996[⊗]

ABSTRACT: An ensemble of $H(CH_2OCH_2)_{12}H$ chains has been studied by molecular dynamics simulations as both melt chains and unperturbed phantom chains as a model system to investigate condensed phase effects on chain conformations of poly(oxyethylene) (POE). In addition, conformations of high molecular weight POE chains in the melt have been determined by small-angle neutron scattering (SANS) experiments over a temperature range of 347−459 K. Our simulations show that POE chains in the melt are more extended than the phantom chains which represent the unperturbed chains in Θ solution. Moreover, the melt chains exhibit a negative temperature coefficient of chain dimensions in contrast to a positive value for the phantom chains. The difference in chain dimensions and the difference in the temperature dependence of chain dimensions between melt and phantom chains are corroborated by the results of our SANS measurements when they are compared with experimental results for POE chains in Θ solution. We attribute these significant deviations in conformational properties of POE chains in the melt from those of unperturbed ideal chains to condensed phase effects, similar to those found in 1,2-dimethoxyethane (DME), a dimer molecule of POE, from both experiments and simulations. That is, simulations show that the population of the C−C−O *gt* conformation is greater in melt chains than in the phantom chains, while the C−C−O $g^{\pm}g^{\mp}$ populations are much smaller in the melt, the latter effect largely accounting for the more extended dimensions of the melt chains. As in DME, the conformation-dependent intermolecular polar attractions (O···H interactions, for example) account for these condensed phase effects, which become more pronounced at lower temperatures. Such intermolecular polar attractions in POE melts also result in increased interatomic packing order, but do not appear to enhance the intermolecular orientational order when compared to simulation results for polymethylene melts.

Introduction

Both the melt and solution properties of poly(oxyethylene) (POE) are of considerable interest for a variety of applications ranging from use as polymer electrolytes to treatment of surfaces for protein adsorption resistance. Many of the desirable properties of POE are undoubtedly related to its conformational characteristics. However, these characteristics, including the role of intermolecular interactions in determining the conformations of POE chains both in the melt and in various solutions, are not well understood.

We have recently performed a quantum chemistry study of the conformational properties of 1,2-dimethoxyethane (DME) as a model (dimer) molecule for POE.[1] Based upon the conformer energies and rotational energy barriers in DME determined from this quantum chemistry study, we have parameterized an accurate force field for DME and POE.[2] Using this force field, we have performed molecular dynamics simulations of gas-phase DME and DME liquids.[3] As has been observed experimentally,[4,5] our simulations revealed strong condensed phase effects in DME. That is, the dominant (*tgt* and $tg^{\pm}g^{\mp}$) conformer populations of DME in the liquid phase were found to differ significantly from those observed in the gas phase. (However, the significance of this condensed phase effect is much less apparent if one considers the gauche fraction of the central C−C bond individually, as in NMR vicinal coupling experiments,[6,7] since the changes in the *tgt* and $tg^{\pm}g^{\mp}$ con-

[⊗] Abstract published in *Advance ACS Abstracts,* March 15, 1996.

S0024-9297(95)01621-4 CCC: $12.00

formers tend to compensate each other.)

The chain dimensions versus molecular weights (M), $\langle R_g^2\rangle/M$, of POE have traditionally been accessed via intrinsic viscosity and light scattering measurements in dilute solutions, where $\langle R_g^2\rangle$ is the mean-square radius of gyration. Many different solvent systems have been used over a temperature range of 25−72 °C. Characteristic ratios C_∞ for high molecular weight samples, given by

$$C_\infty = \langle R^2\rangle_0/nl^2 = 6(\langle R_g^2\rangle_0/M)m_0\, l^{-2} \qquad (1)$$

where $\langle R^2\rangle_0$ is the unperturbed mean-square end-to-end distance, $\langle R_g^2\rangle_0$ is the unperturbed mean-square radius of gyration, n is the number of skeletal bonds, m_0 is the mean molecular weight per skeletal bond, and l^2 (2.1436 Å^2 for POE) denotes the mean-square bond length, typically range from 4 to 5.6.[8−17] Traditional rotational isomeric state (RIS) calculations for unperturbed chains have yielded C_∞ of 4.2 (60 °C)[18] and 5.0 and 5.2 (30 °C).[9,19] The temperature coefficients for chain dimensions, d $\ln\langle R^2\rangle_0$/dT, were calculated[9,19] to be in the range of 0.12×10^{-3} to 0.74×10^{-3} K^{-1}. Our recent quantum chemistry based third-order RIS model[20] for POE, which was parameterized independent of experimental data for the polymer chain dimensions, yields values of $C_\infty = 5.0$ and d $\ln\langle R^2\rangle_0/\mathrm{d}T = 0.11 \times 10^{-3}$ K^{-1}. These values are consistent with experimental values obtained in nonaqueous solvents.[20] However, this characteristic ratio of the unperturbed POE chain is considerably smaller than the value of around 6.9 obtained from the small-angle neutron scattering (SANS) study of polydisperse POE melts at 80 °C by Kugler et al.,[21] indicative of possible condensed phase effects.

In this study, we perform molecular dynamics (MD) simulations of $H(CH_2OCH_2)_{12}H$ chains in the melt and as phantom chains as a model system to investigate possible condensed phase effects in POE, utilizing the quantum chemistry based force field. We have also performed SANS measurements on nearly monodisperse POE melts over a wide temperature range (347−459 K). The difference in chain dimensions between melt and phantom chains found from simulations is compared with that observed between experimental results from POE in Θ solution and our SANS measurements on POE melts. Additionally, we investigate positional and orientational order in POE melts as determined from simulations and compare these results with those obtained from recent simulations of polymethylene melts. We also compare the results of our simulations with the very recent simulation work by Neyertz and Brown,[22] who compared the POE melt chains with the phantom chains for which the intramolecular interactions are truncated at the second order and the third order, respectively, at a fixed temperature of 400 K using different force field parameters.

SANS Studies

Deuterated and protonated forms of POE were prepared by anionic polymerization (Polymer Laboratories, Ltd.). The M_z/M_w and M_w/M_n ratios were around 1.04 as estimated from size exclusion chromatography. Samples were prepared via solution blending with concentrations of 6, 9, 23, and 50 wt % of d-POE in its hydrogenous matrix. The weight-average degree of polymerization (dp) of the d-POE corresponds to an $M_w = 1.06 \times 10^5$ (dp = 2417) for h-POE. The hydrogenous matrix POE had an M_w of 1.1×10^5. Molecular weights were determined via light scattering in dilute solutions.

SANS studies were performed at the NIST cold neutron research facility in Gaithersburg, MD. Scattering profiles for the evaluation of the radius of gyration as a function of temperature were obtained on the 8-m instrument NG-5. Details of the experimental setup and data analysis are described in ref 23. The absolute values of the chain dimensions are subject to errors of a few percent, but the relative change with temperature is better than 0.5%. Table 1 shows the chain dimensions of POE in the melt state from our SANS measurements. Previous SANS results at 353 K[21] yield for a POE sample with a broader polydispersity ($M_z/M_w = 1.5$) a C_∞ of 6.9, a value somewhat higher than ours. Our SANS data, with a C_∞ of about 5.7, indicate chains which are more extended than is found for unperturbed POE chains, for which C_∞ is about 5.0,[20] as discussed above. Moreover, the melt chains show a negative temperature dependence of the chain dimensions, d $\ln\langle R^2\rangle_0/\mathrm{d}T = -0.3 \times 10^{-3}$ K^{-1}, in contrast with the value of about 0.2×10^{-3} K^{-1} from solution viscometric measurements.[24] These results are discussed in greater detail below.

Table 1. Dimensions of POE Melt Chains from SANS Measurements

T (K)	$\langle R_g^2\rangle^{1/2}$ (Å)	$\langle R^2\rangle/M$ (Å^2 mol g^{-1})	C_∞
347	121.3	0.833	5.7
357	121.0	0.829	5.7
371	120.5	0.822	5.6
390	120.0	0.815	5.6
415	119.8	0.812	5.6
440	119.7	0.811	5.5
459	119.5	0.808	5.5

Table 2. Equilibrium Properties of POE Melt Chains

temp (K)	density (g/cm^3)	pressure (atm)	cohesive energy density (10^3 kcal/mol)	$\langle R_g^2\rangle/nl^2$	
				melt	phantom
300	1.122	−62 ± 60	126	0.76	0.57
333	1.094	0 ± 40	116	0.72	
373	1.062	94 ± 35	102	0.67	0.58
450	1.007	163 ± 20	87	0.69	0.59
450[a]		402 ± 80	87		
450[b]		130 ± 80	87		
450[c]		280 ± 50	77		

[a] Dielectric constant of unity. [b] Truncation radius of 13 Å. [c] Dielectric constant of unity, Ewald summation.

Simulation Methodology

The POE simulations were carried out utilizing the quantum chemistry based force field discussed previously[2,3] for a system consisting of 32 chains of 12 repeat units of the structure

$$H-(CH_2OCH_2)_{12}-H$$

Melt simulations were performed at 300, 333, 373, and 450 K at the experimental densities for poly(ethylene glycol) of the same chain length.[25] These densities are given in Table 2. The constant-temperature method of Nosé,[26] as implemented previously,[27] was employed in the simulations. Bond lengths were constrained using the SHAKE algorithm[28] while other internal degrees of freedom (valence angle bends and torsions) remained flexible. A time step of 1 fs was used. The 450 K system was obtained from an initial system consisting of chains on a very low density lattice. The initial system was equilibrated at 600 K for 600 ps. After this time, the

end-to-end vectors for the chains had relaxed and there was no net orientation of chains in the system. The temperature was then decreased to 450 K and the density increased over a 1 ns period. The system was further equilibrated at 450 K for 1 ns. Lower temperature ensembles were equilibrated for 1 ns after reducing the temperature and volume from the next higher temperature during a 200 ps run. The 300 K melt was equilibrated directly from the 373 K ensemble. Sampling time was 2.6 ns at 450 K, 2.0 ns at 373 K, 2.0 ns at 333 K, and 2.4 ns at 300 K. Nonbonded dispersion interactions were truncated at 9 Å, while Coulombic interactions were truncated using the method employed previously to gradually scale the Coulombic force to zero at 9 Å.[27] A distance-dependent dielectric constant was employed as described previously to approximately account for screening effects.[27] Simulations were also performed at 450 K with a dielectric constant of unity in order to investigate the influence of the distance-dependent dielectric constant on $P-V-T$ behavior, chain conformations, and intermolecular order. Two additional simulations at 450 K with a truncation radius of 13 Å (with a distance-dependent dielectric constant) and using standard Ewald summation techniques[29] (dielectric constant of unity), respectively, were performed in order to investigate the influence of the truncation distance on these properties. Simulations were performed on IBM RS/6000 workstations at the NASA Ames Research Center and the IBM Almaden Research Center and on DEC AlphaStation workstations at the University of Missouri—Columbia.

Simulations of phantom chains were performed using the same many-chain ensemble as was used for the melts, but no intermolecular interactions were considered. The same truncation and distance-dependent dielectric constant used in the melt simulations were employed. In order to mimic unperturbed chains in Θ solutions which exhibit only the essential first-, second-, and third-order local interactions,[20] without the effects of long-range interactions which depend on the solvent quality, an atom in a given repeat unit n [$CH_2(\alpha)-O-CH_2(\omega)$] was allowed to interact with atoms within repeat units $n \pm 1$ only, with the following additions. In order to maintain the strong second-order steric interaction between end methylene groups in $CH_2CH_2-O-CH_2CH_2$ g^+g^- conformations, it was necessary to allow the ω-methylene unit of repeat unit n to interact with the α-methylene unit of $n + 2$. Limiting intramolecular interactions, as described above, maintains all important first-, second-, and third-order conformation-dependent interactions. We found that inclusion of additional intramolecular nonbonded interactions for phantom chains up to two entire repeat units ($n \pm 2$) had no significant effect on chain dimensions and conformations, confirming that our phantom chains accurately represent the unperturbed POE chains. When interactions beyond this range were included, the chains began to collapse due to long-range interactions. That is, gas phase chains, where full intramolecular but no intermolecular interactions were employed, were found to collapse due to long-range attractive interactions, reflecting the fact that vacuum is a very poor solvent for these polar chains. For the phantom chain system, equilibration time from the equilibrated melt ensembles was 400 ps and sampling run time was 1.8 ns. Phantom chain calculations were performed at 300, 373, and 450 K. Here, stochastic (Brownian) dynamics simulations[30] with a friction constant of 1/750 fs^{-1} were also carried out and were found to give the same chain conformations and dimensions as MD simulations using the Nosé thermostat. Reported results are for the MD simulations. RIS calculations were also performed for a chain of 12 repeat units at the same temperatures.

Thermodynamic Properties

Pressures and cohesive energy densities (CED) for the melt ensembles were determined at each temperature at experimental densities and are shown in Table 2. In calculating the pressure and CED, standard truncation corrections were included for dispersion interactions. CED values were determined from the intermolecular nonbonded energies. The pressures are reasonable and show only a fairly minor dependence on temperature over a wide temperature range, indicating that the thermal expansion of the system is represented fairly well. At 450 K, the effect of increasing the truncation radius on the pressure is seen to be small; the influence of the distance-dependent dielectric constant on the pressure, using a truncation radius of 9 Å, becomes somewhat larger but the overall effect still remains small. The CED values compare well with an experimental value of $(100 \pm 20) \times 10^3$ kcal/mol for POE at 25 °C.[31] Our value at 300 K is slightly larger than the experimental value. The influence of the distance-dependent dielectric constant on the CED, using a truncation radius of 9 Å, is negligible, as is the effect of increasing the truncation radius to 13 Å. Thermodynamic properties calculated when long-range electrostatic interactions are treated using the Ewald summation method are not very different from those predicted using truncation methods. This agreement is expected for systems with charge-neutral species where at longer separations only dipole−dipole type electrostatic interactions are important. For systems containing charged species (ions), long-range electrostatic interactions are much more important.[29]

Chain Conformations

Mean-Square Radius of Gyration. The mean-square radius of gyration ratio, $\langle R_g^2 \rangle / nl^2$, is reported for our model POE melt and phantom chains in Table 2. The melt chains are more extended than the phantom chains and become more extended as the temperature is lowered. The difference in chain dimensions between melt and phantom chains increases with decreasing temperature. The differences in chain dimensions between melt and phantom chains, where the same force field is used to describe intramolecular interactions, are due to intermolecular interactions in the melt and hence constitute a condensed phase effect, as discussed below.

The characteristic ratio for POE melts (weight average dp = 2417) from our SANS measurements is shown in Figure 1 as a function of temperature. Also shown are RIS[20] predictions for unperturbed chains of the same molecular weight. The C_∞ of the unperturbed high molecular weight RIS chains agrees well with experimental results for unperturbed POE chains in Θ solution[20] and shows a small positive temperature dependence, also in agreement with experimental observations in Θ solutions.[24] The melt chains are extended relative to these unperturbed chains and show a negative temperature dependence, as discussed above. Also shown in Figure 1 are the scaled characteristic ratio for melt and phantom chains from simulations. These values have been scaled to account for the low molecular

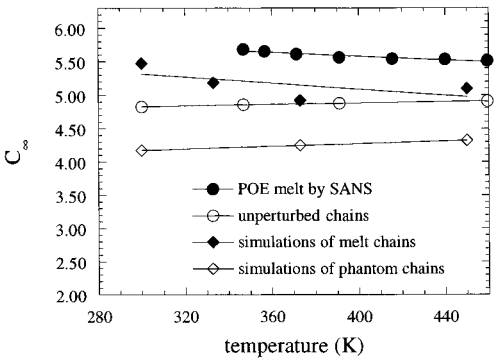

Figure 1. Characteristic ratio of POE as a function of temperature. RIS values are for dp = 2417. Melt and phantom chain simulation values, scaled by use of eq 2, are also shown.

weight of the simulation chains for the purpose of direct comparison with experiment. Values given in Figure 1 were determined from the relationship

$$C_{\infty(\text{scaled})} = 6[\langle R_g^2\rangle/nl^2]_{\text{simulations}} \left[\frac{\langle R_g^2\rangle/n_{\text{dp}=2417}}{\langle R_g^2\rangle/n_{\text{dp}=12}}\right]_{\text{RIS}} \quad (2)$$

The chain length correction is based upon RIS predictions and is found to be independent of temperature. This chain length scaling, ca. 1.2, indicates that the simulated chains are not quite long enough to have reached the asymptotic value for the characteristic ratio. The simulated melt chains are extended relative to the phantom chains, the latter representing the unperturbed chains for our force field. The stimulated phantom chains show a positive temperature dependence of chain dimensions, while the simulated melt chains exhibit a definite trend of negative temperature coefficients, though difficult to quantify due to statistical uncertainty. The differences in the mean-square radius of gyration and its temperature dependence between the simulated melt chains and the phantom chains are similar to those found experimentally between POE chains in the melt and in Θ solution, the latter being well represented by the RIS model chains. Therefore, both experiment and simulation indicate that condensed phase effects are important in determining chain conformations in POE melts.

The discrepancy in chain dimensions between simulated phantom chains and unperturbed RIS model chains arises mainly from small differences in the conformational energies and geometries yielded by the force field and those used in the RIS model. These factors may also explain the fact that the simulated melt chains are slightly more compact than is found from SANS measurements on POE melt chains.

In a very recent paper, Neyertz and Brown reported a comparison of POE chain conformations at 400 K, obtained by MD simulations for melt chains and pivot Monte Carlo simulations for phantom chains, respectively.[22] Their results on POE melt chains with a simulated characteristic ratio $C_\infty \approx 5.5$ is in close agreement with our simulations and SANS experiments. However, they reported a drastic collapse of phantom chains ($C_\infty \approx 1$), when all the intramolecular interactions up to the third-order are considered, whereas their phantom chains including the first-order and second-order interactions only yield $C_\infty \approx 3.8$. In the previous work on a third-order RIS model of POE chains,[20] it was found that explicit inclusion of the third-order interactions for the $CH_2OCH_2CH_2OCH_2$ segments are required for POE chains since the traditional second-order model neglects the significant contribution from the repulsive interactions involving the terminal CH_2 groups in $g^\pm g^\mp g^\pm$ conformations. Inclusion of the third-order interactions was then shown to result in a ca. 20% increase of the characteristic ratio to 5.0, in good agreement with experiments.

Table 3. Conformational Populations for the C−C−O Bond Pair

system	*gt*	$g^\pm g^\mp$	*tt*	*tg*	$g^\pm g^\pm$
450 K melt	**0.451**	**0.154**	**0.205**	**0.096**	**0.094**
450 K phantom	*0.441*	*0.208*	*0.209*	*0.079*	*0.063*
450 K RIS	0.454	0.166	0.201	0.072	0.108
373 K melt	**0.505**	**0.150**	**0.192**	**0.072**	**0.081**
373 K phantom	*0.469*	*0.221*	*0.205*	*0.059*	*0.046*
373 K RIS	0.480	0.172	0.209	0.054	0.086
333 K melt	**0.552**	**0.129**	**0.187**	**0.060**	**0.073**
300 K melt	**0.599**	**0.125**	**0.166**	**0.045**	**0.064**
300 K phantom	*0.494*	*0.232*	*0.206*	*0.038*	*0.030*
300 K RIS	0.508	0.176	0.220	0.030	0.060

Table 4. Conformational Populations for the C−O−C Bond Pair

system	*tt*	*tg* + *gt*	$g^\pm g^\mp$	$g^\pm g^\pm$
450 K melt	**0.400**	**0.506**	**0.026**	**0.067**
450 K phantom	*0.404*	*0.489*	*0.033*	*0.073*
450 K RIS	0.403	0.500	0.018	0.078
373 K melt	**0.457**	**0.475**	**0.018**	**0.050**
373 K phantom	*0.432*	*0.480*	*0.025*	*0.062*
373 K RIS	0.451	0.476	0.011	0.063
333 K melt	**0.521**	**0.430**	**0.012**	**0.037**
300 K melt	**0.565**	**0.397**	**0.009**	**0.030**
300 K phantom	*0.460*	*0.472*	*0.016*	*0.051*
300 K RIS	0.509	0.438	0.005	0.047

In this regard, the consequence of including all the third-order interactions for the phantom chains in ref 22 is completely opposite to the conclusion of ref 20. Neyertz and Brown attributed this difference to the abundant $g^\pm g^\mp g^\pm$ $CH_2CH_2OCH_2CH_2O$ conformers stabilized by the third-order $CH_2\cdots O$ attractions according to their force field parameters. The stability of such conformers was excluded in ref 20 due to the high energies of the first- and second-order repulsions in the $g^\pm g^\mp$ $CH_2CH_2OCH_2CH_2$ conformations. This has been corroborated by our phantom chain simulations including interactions up to ($n \pm 2$) CH_2OCH_2 segments as discussed above. Moreover, our separate quantum chemical calculations to check the stability of the $g^\pm g^\mp g^\pm t$ conformer of the $CH_3CH_2OCH_2CH_2OCH_3$ molecule did not show any such low-energy minimum. In addition, Miyasaka et al. previously carried out molecular mechanics calculations on $CH_3CH_2OCH_2CH_2OCH_2CH_3$ molecule and concluded that the conformations containing more than two consecutive gauche states were found to be higher in energy.[32] Therefore, the surprising results of ref 22 indicate that the force fields employed therein are grossly overestimating the electrostatic attractions or underestimating the unfavorable torsional energies or the steric repulsions in the $g^\pm g^\mp g^\pm$ $CH_2CH_2OCH_2CH_2O$ conformations and thus cast doubt on the melt chain results as well.

Pairwise Conformational Populations. The populations of conformational pairs for C−C−O conformations and C−O−C conformations for melt, phantom, and RIS chains are given in Tables 3 and Tables 4, respectively. The gauche (g^+ and g^-) states are $60° \le g^+ < 180°$ and $180° \le g^- < 300°$. The C−C−O *gt* ($g^+t + g^-t$), $g^\pm g^\mp$, and *tt* populations are shown as a function of temperature in Figure 2. For the C−C−O pair, the *gt* population is greater for melt chains than phantom or

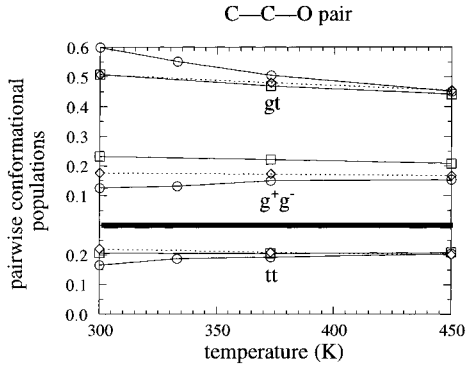

Figure 2. Conformational pair populations for the C−C−O bond pair in POE as a function of temperature. Circles are melt chains, squares are phantom chains, and diamonds are RIS model chains.

RIS chains at 300 and 373 K. At 450 K, the difference in *gt* populations is smaller. Conversely, the $g^{\pm}g^{\mp}$ population is lower in the melt chains than phantom or RIS chains, with the difference increasing with decreasing temperature. A similar trend can be seen for the *tt* conformations. At lower temperature, these differences in conformation between melt chains and phantom chains are consistent with differences in conformations observed in the model dimer, DME, between the liquid and gas phases, both experimentally[4,5] and in our recent simulation study.[3] At room temperature, the *tgt* population in DME is significantly higher in the liquid phase than in the gas phase, while the $tg^{\pm}g^{\mp}$ population is significantly greater in the gas phase than in the liquid phase. The *ttt* population was somewhat greater in the gas phase. We attributed the increase in *tgt* population and decrease in *ttt* population in the liquid to intermolecular polar interactions, which favor conformers with large dipole moments. These same considerations would account for the greater *gt* and smaller *tt* C−C−O pair populations seen in the POE melts compared with phantom chains.

We believe the decrease in the $tg^{\pm}g^{\mp}$ conformer in DME liquid to be due to strong intermolecular electrostatic O···CH interactions, which compete with the intramolecular O···CH interactions which stabilize the $tg^{\pm}g^{\mp}$ conformer.[3] We have plotted the intermolecular O···H and O···C pair distribution functions for POE melt chains in Figure 3. As in DME,[3] there are shoulders in the O···H pair distribution functions which begin at separations of less than 3 Å. These separations are consistent with the intramolecular 1,5 CH···O distance of 2.6 Å seen in the $tg^{\pm}g^{\mp}$ conformer of DME from ab initio calculations.[1] The shoulder becomes much better resolved at lower temperature. Again, as in DME, there are shoulders in the C···O pair distribution functions between 3 and 4 Å, consistent with the intramolecular 1,5 CH···O distance of 3.2 Å seen in the $tg^{\pm}g^{\mp}$ conformer of DME from ab initio calculations.[1] We conclude that, as in DME, strong electrostatic intermolecular CH···O interactions are present in POE melts. These intermolecular interactions occur to some extent at the expense of the 1,5 CH···O intramolecular interactions, accounting for the observed difference in the C−C−O $g^{\pm}g^{\mp}$ population between the melt and phantom chains. The contribution of these interactions increases with decreasing temperature; this behavior explains the observed increase in the difference between melt chain and phantom or RIS chain C−C−O $g^{\pm}g^{\mp}$ populations with decreasing temperature.

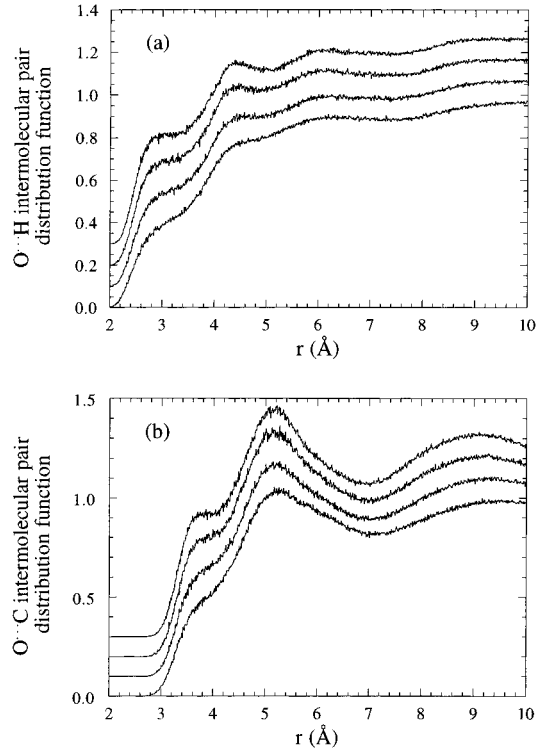

Figure 3. Intermolecular (a) O···H and (b) O···C pair distribution functions for POE melts as a function of separation distance. For clarity, functions obtained at different temperatures have been offset along the ordinate by 0.0 (450 K), 0.1 (373 K), 0.2 (333 K), and 0.3 (300 K).

For the C−O−C pair populations, the most dramatic difference between melt and phantom chains is found for the *tt* population. The C−O−C *tt* population for the melt chains shows a much stronger dependence on temperature than seen in phantom or RIS chains, with the population increasing with decreasing temperature. This is primarily the result of the increase in the C−C−O *gt* and the decrease in the C−O−C $g^{\pm}g^{\mp}$ population with decreasing temperature discussed above.

It was found that increasing the Coulombic truncation distance from 9 to 13 Å had little influence on any of the pairwise populations (less than a 5% change for any pair). Employing a dielectric constant of unity had a slightly larger effect (but still less than a 10% change for any pair) due to changes in intramolecular interactions. Effects of this magnitude were seen in simulations of gas phase DME.[3] Pairwise populations determined using the Ewald summation technique were the same as those obtained using a spherical truncation and a dielectric constant of unity.

Melt Structure

Atomic Pair Distribution Functions. Melt structure was examined by looking at both positional and orientational order. The C···C and O···O intermolecular pair distribution functions are shown in Figure 4. The first peak in these pair distribution functions occurs between 4 and 5 Å and is indicative of nearest-neighbor chain packing. The distance is less than that seen for the first peak in the C···C pair distribution function in *n*-$C_{13}H_{28}$[30,33] and *n*-$C_{44}H_{90}$,[34] where the peak occurs at distances greater than 5 Å. The closer chain packing in POE reflects the greater density of the POE systems. The height of the first peak in the C···C distribution is greater in POE melts than was observed in polymeth-

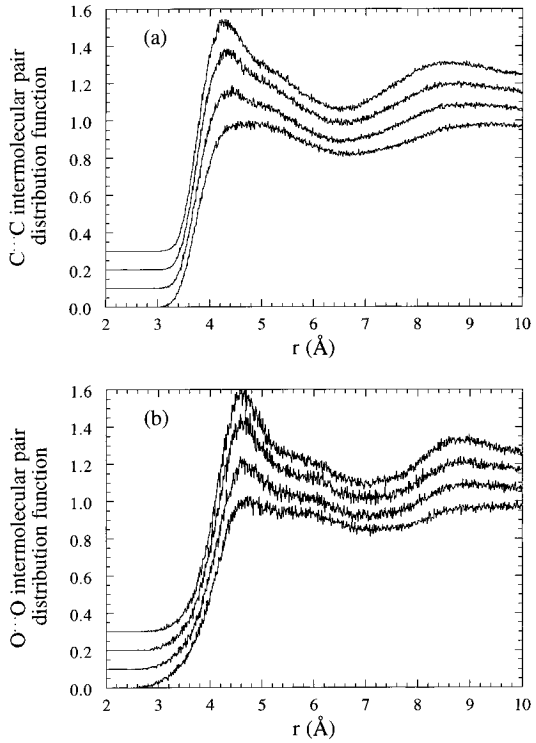

Figure 4. Intermolecular (a) C···C and (b) O···O pair distribution functions for POE melts as a function of separation distance. For clarity, functions obtained at different temperatures have been offset along the ordinate by 0.0 (450 K), 0.1 (373 K), 0.2 (333 K), and 0.3 (300 K).

ylene melts and shows a greater increase with decreasing temperature. At 450 K, the first C···C and O···O peaks in POE are broad and poorly resolved. With decreasing temperature, these broad peaks resolve into much sharper peaks with shoulders between 5 and 6 Å. The emerging structure in the pair distribution functions with decreasing temperature indicates increasing regularity in the interchain packing for nearest neighbors, perhaps reflecting strong CH···O intermolecular interactions as discussed above.

Intermolecular Charge Distribution Functions. It is possible to calculate an intermolecular charge distribution function for each atom type *i* by weighting the corresponding intermolecular atomic pair distribution functions (*ij*) by the appropriate atomic charge and relative number density for each atom type *j*. The intermolecular oxygen−charge distribution function is shown in Figure 5. The radial charge density about an oxygen atom is given by multiplying the charge distribution function by the density of monomer units. A large positive charge peak is seen in the distribution at just under 3 Å, the distance corresponding to the shoulder in the intermolecular O···H pair distribution function (Figure 3a). The peak height increases significantly with decreasing temperature. This peak confirms the presence of intermolecular O···H Coulombic interactions which, as discussed earlier, strongly influence local chain conformations in the condensed phase. The negative charge peak at around 5 Å reflects the nearest-neighbor interchain backbone−backbone interactions. Little charge structure is seen at the second-neighbor chain separation or beyond at the higher temperatures. Minor structure can be seen at the lower temperatures.

As a test of the influence of the distance-dependent dielectric constant and the influence of the Coulombic

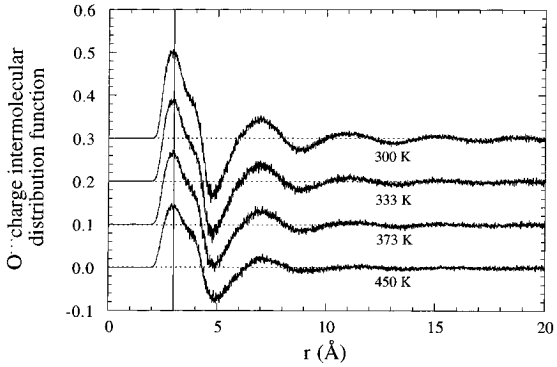

Figure 5. Intermolecular oxygen−charge distribution functions for POE melts as a function of separation distance. For clarity, functions obtained at different temperatures have been offset along the ordinate by 0.0 (450 K), 0.1 (373 K), 0.2 (333 K), and 0.3 (300 K).

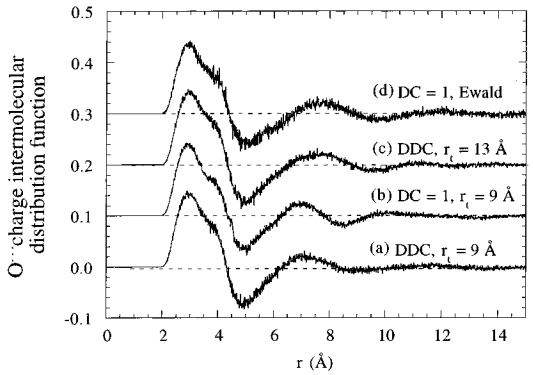

Figure 6. Intermolecular oxygen−charge distribution functions for POE melts as a function of separation distance at 450 K. Curve a: with a distance-dependent dielectric constant, truncation radius of 9 Å. Curve b: with a dielectric constant of unity, truncation radius of 9 Å, offset along the ordinate by 0.1. Curve c: with a distance-dependent dielectric constant, truncation radius of 13 Å, offset along the ordinate by 0.2. Curve d: with a dielectric constant of unity, Ewald summation, offset along the ordinate by 0.3.

truncation distance on intermolecular structure, the oxygen−charge intermolecular distribution functions at 450 K for truncation distances of 9 Å (a) and 13 Å (c), with a truncation of 9 Å employing a dielectric constant of unity (b), and using the Ewald summation technique for electrostatic interactions (d) are shown in Figure 6. For separations less than 5 Å, the distribution functions a and c are nearly indistinguishable, and distributions b and d do not differ significantly from these. At separations greater than 6 Å, the influence of the truncation radius is seen. For a and b, the second positive charge peak is shifted by about 0.5 Å to smaller separation compared to c. This shift is due to the fact that the Coulombic forces are reduced to zero at the truncation radius. The effect is greater for b, where the unit value of the dielectric constant results in stronger electrostatic forces. It is worth noting that even for a truncation radius of 13 Å or for the Ewald summation results, where no truncation is employed for the electrostatic interactions, little structure is seen in the charge distribution beyond the second-neighbor distance of 10 Å. For the individual pair distribution functions, the distance-dependent dielectric constant and truncation distance have a significant influence on the O···O pair only. This is consistent with the relatively large partial atomic charge associated with the oxygen atom, making this by far the strongest individual pairwise Coulombic interaction. The differences seen in the

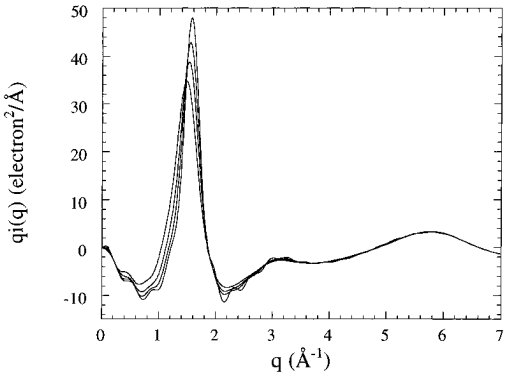

Figure 7. Reduced X-ray scattering intensity from POE melts as a function of the scattering vector. The curves are for POE melts at 300, 333, 373, and 450 K, with the height of the first intermolecular peak decreasing with increasing temperature.

Table 5. Characteristics of the Intermolecular X-ray Scattering Intensity Peak as a Function of Temperature

property	300 K	333 K	373 K	450 K
q_{max} (Å^{-1})	1.56	1.53	1.50	1.45
FWHM[a] (Å^{-1})	0.36	0.41	0.46	0.53

[a] Full width of diffraction peak at half-maximum intensity.

oxygen−charge distribution functions in Figure 6 can be attributed mostly to differences in the O···O pair distribution functions.

X-ray Scattering. The calculated reduced X-ray scattering intensity

$$qi(q) = q[I(q) - \langle f(q)^2 \rangle] \tag{3}$$

as a function of the scattering vector q is shown in Figure 7. Here, $q = 4\pi\sin\theta/\lambda$, where λ is the wavelength of the scattered radiation, 2θ is the scattering angle, $I(q)$ is the scattering intensity per atom, and $\langle f(q)^2 \rangle$ is the atomic scattering function squared averaged over all atoms. The characteristics of the intermolecular X-ray scattering peak are given in Table 5. The intermolecular scattering peaks occur at q values between 1.45 and 1.6 Å^{-1}, significantly greater than the 1.25−1.4 Å^{-1} seen in n-$C_{13}H_{28}$[30,33] and n-$C_{44}H_{90}$.[34] This closer chain packing in POE reflects the higher density of the system. Both Figure 7 and Table 5 indicate that the intermolecular scattering peak narrows considerably over the temperature range studied, much more than was seen in the polymethylene systems over the same temperature range. We are currently conducting X-ray scattering experiments for POE melts, with which direct comparison of simulations will be made.

Orientation Correlation. Orientational order in POE melts was investigated by calculating the intermolecular orientation correlation function for two-bond segments, given by

$$S(r) = \frac{1}{2}[3\langle \cos^2 \beta(r) \rangle - 1] \tag{4}$$

where β is the angle formed by the vectors (one for each two-bond segment) bisecting the bonds forming the segment and r is the distance between the centers of the bisecting vectors. The intermolecular orientation correlation functions, multiplied by the two-bond segment pair distribution function $G(r)$, are shown in Figure 8. The first peaks occur about 4.5 Å, a smaller separation than was seen in polymethylenes.[30,34] The height of the first peak in the POE orientational pair distribution function increases with decreasing temperature, indicating an increase in orientational order. Unlike positional order, however, the temperature dependence of the orientational order in POE melts does not appear to be significantly greater than was seen for polymethylene melts. At 300 K, the POE peak height is comparable to that seen in n-$C_{13}H_{28}$ at 312 K. These results indicate that the intermolecular O···CH interactions which lead to greater positional order in POE melts as compared to polymethylenes do not result in enhanced intermolecular orientational order of local chain segments.

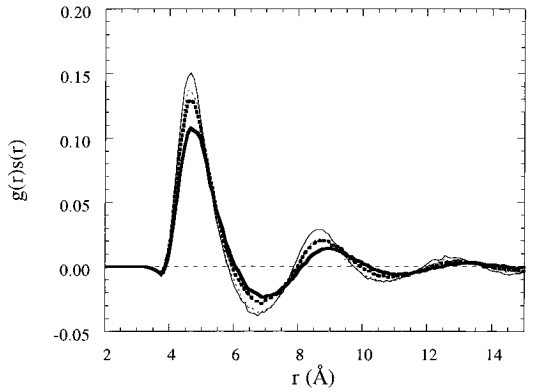

Figure 8. Weighted intermolecular orientational correlation function as a function of separation for two-bond segments in POE melts. The curves are for POE melts at 300, 333, 373, and 450 K, with the height of the first intermolecular peak decreasing with increasing temperature.

Conclusions

Comparison of pairwise conformational populations for POE chains determined from simulations of the melt and the phantom chains indicates that condensed phase effects, similar to those seen in the model dimer, 1,2-dimethoxyethane (DME), are also present in POE. The C−C−O gt population is greater in melt chains than in phantom or unperturbed chains, while the C−C−O $g^{\pm}g^{\mp}$ population is much smaller in the melt. The condensed phase effects become more pronounced as the temperature decreases. These effects lead to melt chains which are more extended compared to unperturbed chains, with a negative temperature dependence of the chain dimensions, in agreement with SANS measurements of the mean-square radius of gyration of POE melts as a function of temperature. The intermolecular O···CH interactions, which compete with the intramolecular O···CH attractions that stabilize the C−C−O $g^{\pm}g^{\mp}$ conformation, have been shown to account for the lower C−C−O $g^{\pm}g^{\mp}$ population in the melt. The effect of such intermolecular O···CH interactions becomes more pronounced at lower temperatures, thereby leading to the negative temperature coefficient of chain dimensions for POE melt chains in contrast to the positive value for the unperturbed POE chains in Θ solution. Compared to polymethylene melts, the strong, specific intermolecular O···CH interactions appear to result in increased intermolecular positional order but not orientational order.

The origin of the condensed phase effects of POE chains is believed to be the fact that the intermolecular (attractive) interactions are strongly dependent on the local conformations of POE chain segments. This situation is in stark contrast to the case of simple hydrocarbon polymers such as polyethylene, for which there exist no conformation-dependent intermolecular attractions, and no condensed phase effect has been seen by

SANS experiments[35−37] as well as recent MD simulations.[38] In this regard, it should be noted that Flory's prediction of unperturbed random coils in bulk amorphous polymers is based on the assumption that interactions between chain segments belonging to different molecules are completely independent of local chain conformations.[39] Hence, our finding of significant condensed phase effects in POE melts shows that one should be careful in generalizing Flory's unperturbed random-coil model to all bulk amorphous polymers and concentrated polymer solutions. That is, one needs to consider the nature and the consequence of conformation-dependent intermolecular (attractive) interactions which may exist in various polymer systems.

Acknowledgment. G.D.S. would like to acknowledge support from NASA through Eloret Contract NAS2-14031.

References and Notes

(1) Jaffe, R. L.; Smith, G. D.; Yoon, D. Y. *J. Phys. Chem.* **1993**, *97*, 12745.
(2) Smith, G. D.; Jaffe, R. L.; Yoon, D. Y. *J. Phys. Chem.* **1993**, *97*, 12752. Please note that eq 7 of this paper should be

$$E^t(\phi_{ijkl}) = \sum_{n=1}^{3} \frac{1}{2} k^t_{ijkl}(n)[1 - \cos\, n(\phi_{ijkl} - \phi^0_{ijkl}(n))]$$

(3) Smith, G. D.; Jaffe, R. L.; Yoon, D. Y. *J. Am. Chem. Soc.* **1995**, *117*, 530.
(4) Astrup, E. E. *Acta Chem. Scand.* **1979**, *A33*, 655.
(5) Yoshida, H.; Kaneko, I.; Matsuura, H.; Ogawa, Y.; Tasumi, M. *Chem. Phys. Lett.* **1992**, *196*, 601. Ogawa, Y.; Ohta, M.; Sakakibara, M.; Matsuura, H.; Harada, I.; Shimanouchi, T. *Bull. Chem. Soc. Jpn.* **1977**, *50*, 650.
(6) Tasaki, K.; Abe, A. *Polym. J.* **1985**, *17*, 641.
(7) Inomata, K.; Abe, A. *J. Phys. Chem.* **1992**, *96*, 7932.
(8) Bailey, F. E.; Callard, R. W. *J. Appl. Polym. Sci.* **1959**, *1*, 56.
(9) Abe, A.; Mark, J. E. *J. Am. Chem. Soc.* **1976**, *98*, 6468.
(10) Beech, D. R.; Booth, C. *J. Polym. Sci., Part A-2* **1969**, *7*, 575.
(11) Boucher, E. A.; Hines, P. M. *J. Polym. Sci., Polym. Phys. Ed.* **1978**, *16*, 506.
(12) Ataman, M.; Boucher, E. A. *J. Polym. Sci., Polym. Phys. Ed.* **1982**, *20*, 1585.
(13) Wolff, C. *Can. J. Chem. Eng.* **1980**, *58*, 654.
(14) Amu, T. C. *Polymer* **1982**, *23*, 1775.
(15) Allen, G.; Tanaka, T. *Polymer* **1978**, *19*, 271.
(16) Allen, G.; Booth, C.; Hust, S. J.; Jones, M. N.; Price, C. *Polymer* **1967**, *8*, 391.
(17) Allen, G. *Proc. R. Soc. London, Ser. A* **1976**, *351*, 385.
(18) Yoon, D. Y.; Flory, P. J. *Macromolecules* **1976**, *9*, 294.
(19) Abe, A.; Tasaki, K.; Mark, J. E. *Polym. J.* **1985**, *17*, 883.
(20) Smith, G. D.; Yoon, D. Y.; Jaffe, R. L. *Macromolecules* **1993**, *26*, 5213.
(21) Kugler, J.; Fischer, E. W.; Peuscher, M.; Eisenbach, C. D. *Makromol. Chem.* **1983**, *184*, 2325.
(22) Neyertz, S.; Brown, D. *J. Chem. Phys.* **1995**, *102*, 9725.
(23) Balsara, N. P.; Fetters, L. J.; Hadjichristidis, N.; Lohse, D. J.; Han, C. C.; Graessley, W. W.; Krishnamoorti, R. *Macromolecules* **1992**, *25*, 61.
(24) Bluestone, S.; Mark, J. E.; Flory, P. J. *Macromolecules* **1974**, *7*, 325.
(25) Becht, V. J.; Hellwege, K. H.; Knappe, W. *Kolloid-Z. Z. Polym.* **1967**, *216*, 150. The 450 K value is an extrapolation from lower temperature data.
(26) Nosé, S. *J. Chem. Phys.* **1984**, *81*, 512.
(27) Smith, G. D.; Jaffe, R. L.; Yoon, D. Y. *Macromolecules* **1993**, *26*, 298.
(28) Ryckaert, J. P.; Ciccotti, G.; Berendsen, H. J. C. *J. Comput. Phys.* **1977**, *23*, 327.
(29) Allen, M. P.; Tildesley, D. J. *Computer Simulations of Liquids*; Clarendon Press: Oxford, 1987.
(30) Yoon, D. Y.; Smith, G. D.; Matsuda, T. *J. Chem. Phys.* **1993**, *98*, 10037.
(31) Brandrup, J.; Immergut, E. H. *Polymer Handbook*; John Wiley and Sons: New York, 1989.
(32) Miyasaka, T.; Yoshida, T.; Imamura, Y. *Makromol. Chem.* **1983**, *184*, 1285.
(33) Smith, G. D.; Yoon, D. Y. *J. Chem. Phys.* **1994**, *100*, 649.
(34) Smith, G. D.; Yoon, D. Y.; Zhu, W.; Ediger, M. D. *Macromolecules* **1994**, *27*, 5563.
(35) Lieser, G.; Fischer, E. W.; Ibel, K. *J. Polym. Sci., Polym. Lett. Ed.* **1975**, *13*, 39.
(36) Schelten, J.; Ballard, D. G.; Wignall, G. D.; Longman, G.; Schmatz, W. *Polymer* **1976**, *17*, 751.
(37) Boothroyd, A. T.; Rennie, A. R.; Boothroyd, C. B. *Europhys. Lett.* **1991**, *15*, 715.
(38) Han, J.; Jaffe, R. L.; Yoon, D. Y., in preparation.
(39) Flory, P. J. *Proc. R. Soc. London, A* **1956**, *234*, 60; *J. Macromol. Sci., Phys.* **1976**, *B12*, 1; *Ber. Bunsenges. Phys. Chem.* **1977**, *81*, 885.

MA951621T